Nonlinear time-dependent density-functional-theory study of ionization and harmonic generation in CO_2 by ultrashort intense laser pulses: Orientational effects

Emmanuel Penka Fowe and Andre D. Bandrauk*

Laboratoire de Chimie Théorique, Faculté des sciences and Université de Sherbrooke, Quebec, Canada, J1K 2R1

(Received 17 September 2009; published 16 February 2010)

Time-dependent density-functional-theory (TDDFT) methods are used to calculate the orientational dependence of ionization and molecular high-order harmonic generation (MHOHG) in the CO_2 molecule as a function of laser intensity $I_0 \geqslant 10^{14}$ W/cm^2 for few-cycle 800 nm laser pulses. A time-series analysis is used to confirm the recollision model in MHOHG for different density potentials. It is found that at intensities $I_0 > 3.5 \times 10^{14}$ W/cm^2, lower highest occupied molecular orbitals (HOMO's) contribute significantly to ionization and to the MHOHG process. This is due to the symmetry of these orbitals. Even though such lower orbitals have higher ionization potentials (IP), ionization and MHOHG processes occur when orbital densities are maximum with laser polarization direction.

DOI: 10.1103/PhysRevA.81.023411 PACS number(s): 33.20.Xx, 33.80.Rv, 33.80.Wz, 33.90.+h

I. INTRODUCTION

Current progress in intense ultrashort laser technology allows for the study of highly nonlinear phenomena such as high-order harmonic generation (HHG) and above threshold ionization (ATI) in atoms [1]. Molecular high-order harmonic generation [2] (MHOHG) is a new area of research due to the multicenter nature of interferences in MHOHG processes [3] and also in molecular ATI itself [4]. Nonperturbative interference effects are an essential signature in new applications such as laser-induced electron diffraction (LIED) [4] and molecular orbital tomography [5]. The nonlinear nonperturbative response of molecules to intense ultrashort laser pulses necessitates the development of nonperturbative numerical methods to solve problems of interactions with intense laser pulses. The first step is accurate numerical solutions of the time-dependent multidimensional Schrödinger equation (TDSE) followed by propagation of pulses in molecular media through Maxwell's equations [6].

In the present work, we focus on time-dependent density-functional-theory (TDDFT) methods as one tool for studying nonlinear nonperturbative response of molecules to intense ultrashort laser pulses [7]. As an example, simple TDDFT functionals were used to characterize pulses by interaction with metal surfaces [8]. Density-functional theory has become a ubiquitous method of solving ground-state electronic problems in atoms and molecules [9]. The extension to nonperturbative time-dependent phenomena has emerged by the existence of a rigorous theorem relating the exact time-dependent density to external time-dependent potentials [10]. Our previous work on the one-electron H_2^+ system showed that the orientation dependence of ionization in such a system allows for the direct imaging of molecular orbitals [11]. MHOHG was used for tomographic imaging of orbitals in the N_2 molecule [5]. In such tomographic imaging, the first step is ionization followed by recollision of the electron with the parent ion [12–14]. As we emphasized previously [2,11], a rigorous description of the first ionization step is a prerequisite in developing MHOHG as a tomographic tool for imaging molecular orbitals. In the present work, we study through numerical solutions of Kohn-Sham (KS) equations in TDDFT [7] the ionization process to establish the individual contributions of molecular orbitals (MO's) as a function of intensity and orientation. Earlier experiments on ionization of ethylene, C_2H_4, by intense short pulses showed the occurrence from orbitals below the HOMO with higher ionization potentials [11]. In the next step, we use a time-series analysis [2,11,12] to examine the validity of the recollision model in MHOHG for the three-center system, CO_2. MHOHG in this system was recently studied thoroughly experimentally by using transient alignment techniques using low-frequency IR lasers [14–16]. Theoretically, the CO_2 molecule was recently treated [17] in the strong-field approximation (SFA) [18]. In the present work, we calculate the contribution of each MO to the ionization and MHOHG process by TDDFT methods.

II. NONLINEAR TDDFT AND KOHN-SHAM EQUATIONS

To calculate the ionization probabilities, the first step in the recollision model [12,19], leading to MHOHG, we adopt the KS orbital method [20] for modeling the nonlinear nonperturbative response of molecules to ultrashort intense laser fields [7]. The TDDFT method provides the most detailed and feasible *ab-initio* approach for tackling many-body problems. Density-functional theory, as first introduced by Hohenberg and Kohn [9] and extended by Kohn and Sham [20], is based on the existence of an exact mapping between the one-particle density and external potentials. This leads to the density of the interacting system being obtained from the density of an auxiliary system of noninteracting particles moving in an effective local single-particle potential. A time-dependent generalization of DFT, TDDFT, was provided by Runge and Gross [10] showing that there is a one-to-one correspondence between the external (time dependent) potential, $\upsilon_{;\mathrm{ext}}(r,t)$, and the time-dependent one-electron density, $n(r,t)$, for many-body systems evolving from a fixed initial state. The time-dependent electronic density for the closed-shell system is

$$n(r,t) = \sum_{\sigma=\uparrow,\downarrow} n_\sigma(r,t) = \sum_{\sigma=\uparrow,\downarrow} \sum_{i}^{N_\sigma} |\psi_{i\sigma}(r,t)|^2, \qquad (1)$$

*Canada Research Chair; andre.bandrauk@usherbrooke.ca

where $N_\sigma = N_\downarrow, N_\uparrow$ is the number of occupied orbitals for a given spin σ,$\psi_{i\sigma}(r,t)$ is the occupied orbital obtained through the time-dependent KS equations (in a.u.)

$$i\frac{\partial}{\partial t}\psi_{i\sigma}(r,t) = \left[-\frac{1}{2}\nabla^2 + \upsilon_{\text{eff}}(r,t)\right]\psi_{i\sigma}(r,t), \qquad (2)$$

where

$$\upsilon_{\text{eff}}(r,t) = \upsilon_{\text{ext}}(r,t) + \upsilon_h(r,t) + \upsilon_{xc,\sigma}(r,t). \qquad (3)$$

The first term is the external potential due to the interaction of the electron with an external laser field and the nuclei while the second term accounts for the classical Hartree electrostatic interaction between electrons; the third term, the exchange-correlation potential, includes all nontrivial many-body effects and has an extremely complex (and essentially unknown) functional dependence on the density. This dependence can be nonlocal both in space and in time, thus, the quality of numerical solutions of Eq. (2) will depend on the quality of the approximation to the *xc* potential used. However, recent theoretical work demonstrated that for low frequency, nonresonant multiphoton processes an adiabatic approximation, where all potentials are local, is an adequate approximation [21]. When an intense electric low-frequency field is applied on a molecule, it tries to displace the electrons out by ionization; thus, the highest ionization potential (IP) or barriers will hinder this electronic displacement much more than lower IP or barriers. Therefore, the choice of an approach that accurately reproduces the experimental IP is useful for our analysis. DFT and Hartree-Fock (HF) approaches were first used for comparison. For HF, the IP is computed using the simplest treatment based on Koopman's theorem [22], which states that the IP is given by the negative restricted (closed shell) HF orbital energy (-ε_i), calculated in the neutral system. This approach ignores the relaxation of the molecular orbitals after the ionization. However, this effect tends to be canceled by the absence of the electron correlation in the HF wave function [23]. In DFT, Koopmans' theorem is not explicitly applicable, but the eigenvalue of the highest KS orbital was proved by Janak [24] to be the physical IP if the functional is exact. For this work, we use the local-density approximation (LDA), which was widely used in strong fields [7] due to its simplicity and applicability to various systems with relatively less time-computational cost. However, LDA is constructed from the homogenous gas systems and suffers for the wrong asymptotic behavior originating from the incomplete cancellation of the self-interactions. For these reasons, we also use for comparison the Van Leeuwen and Baerends [25] potential, LB94, $\nu_x^{\sigma\,\text{LB94}}(\mathbf{r}) = \nu_x^{\text{LDA}}(\mathbf{r}) - \beta n_\sigma^{1/3}(\mathbf{r})\frac{x_\sigma^2}{1+3\beta x_\sigma \ln(x_\sigma+\sqrt{(x_\sigma^2+1)})}$ where $x_\sigma = \frac{|\nabla n_\sigma(\mathbf{r})|}{n_\sigma(\mathbf{r})^{4/3}}$; $\beta = 0.05$, which introduces a gradient correction to LDA exchange correlation so as to reproduce the Coulomb asymptotic behavior of the potential. A convenience of the LB94 potential lies in its explicit dependency on the local density and its gradient. This potential yields good estimates of the IP for atoms and small molecules, especially in the framework of the linear response TDDFT excitation energy [26]. This model potential significantly corrects the higher moments of the density, notably for diffuse outer orbitals involved in excitations, and in our case, ionization. The LB94 also includes partial and considerable self-interaction correction (SIC) resulting from an interaction of an electron with itself, of importance to electronic transport [27]. Such corrections are known to produce spurious oscillations in photoionization calculations, [28] but little is known about the corrections for strong fields in the nonpertubative regime. Our results show that the LB94 potential offers accurate IP's for all orbitals; an essential starting point for accurate ionization.

III. COMPUTATIONAL METHODS

In the present work, the TDDFT-KS equation, Eq. (2), was discretized in space using finite-difference (FD) grid techniques. For numerical reasons we represent the electron-ion interaction by the norm conserving nonlocal Troullier-Martins pseudopotential [29], which allows us to explicitly treat many fewer electrons and to avoid the fast oscillations produced by the core electrons. The pseudopotentials are generated such that the pseudo-wave functions imitate the all-electron atomic wave functions. The CO bond length is set to its experimental [30] value, CO = 0.1162 nm and the CO_2 molecule is placed in a large three-dimensional (3D) cubic grid cell [atomic units (au) are used] of dimension $|z_{\max}| = 40$ au (1 au = 0.0529 nm). The uniform FD grid spacing $\Delta z = 0.28$ au was used and the convergence of the calculations was checked against results making use of a smaller grid spacing. The size of the grid is determined by the maximum radius $\alpha = E_0/m\omega^2$ of an electron in a time-dependent electric field of maximum amplitude E_0. Thus at $E_0 = 0.1$ au corresponding to an intensity $I_0 = 3.50 \times 10^{14}$ W/cm^2 (1 au: $I_0 = 3.50 \times 10^{16}$ W/cm^2, $E_0 = 5 \times 10^9$ V/cm), $\alpha = 30$ au at $\lambda = 800$ nm, $\omega = 0.057$ au. The external potential created by an intense laser field is assumed to arise from an oscillating electric field with a cosine envelope. When the laser is polarized parallel to the molecular axis z, $\upsilon_{\text{ext}}(r,t)$ is given by

$$\upsilon_{\text{ext}}(r,t) = zE_0\cos^2\left(\frac{\pi t}{T}\right)\sin(\omega t)(0 \prec t \prec T), \qquad (4)$$

where T determines the laser pulse duration. The laser intensity is related to the field strength by $I = \frac{1}{2}\varepsilon_o c E_0^2$, ε_o is the permittivity of free space and c is the speed of light. The angle θ, between the linear polarized laser and the main molecular axis varies from 0 to 90°. The total area condition $\int_{-\infty}^{+\infty} E(t)dt = o$ is verified to ensure no spurious static effects [1,2]. The time-dependent equations in Eq. (2) are solved using the Crank-Nicholson scheme [19] with $\Delta t = 0.02$ au (1 au = 24×10^{-18} s) as the time step. All calculations were done using eight optical cycles pulse duration.

A. Orbital ionization

To absorb the ionized charge density and avoid reflections at the boundary of the box due to ionization during the propagation we employ a mask function. By using this technique, the KS wave function is multiplied in each time step by a function $M(z)$ which is 1 in the inner simulation region and gradually goes to 0 at the borders. The masking

function in one dimension is defined as

$$M(z) = \begin{cases} \sin^{\frac{1}{4}}\left(\frac{z_{\max}-|z|}{2a}\pi\right), & (z_{\max} - |z| \prec a), \\ 1 & (\text{otherwise}). \end{cases} \quad (5)$$

$z_{\max} = 40$ au is the extension of the box in the z direction, $a = 6$ au is the width of the mask function. It is assumed that the electrons in the $z_{\max} \succ |z|$ domain are completely ionized and cannot return to the nuclei. A different approach to removing outgoing flux density consists in adding an imaginary potential [31], which causes an exponential decay of the wave function or in using the exterior complex scaling coordinate transformation as the absorbing boundary [32]. The time-dependent ionization probability, $P_{i,\sigma}(t)$, of an individual spin orbital is calculated as [7]

$$P_{i,\sigma}(t) = 1 - N_{i,\sigma}(t), \quad (6)$$

where $N_{i,\sigma}(t) = \langle\psi_{i,\sigma}(r,t)|\psi_{i,\sigma}(r,t)\rangle$ is the time-dependent population (survival probability) of the i,σth spin population.

B. Harmonic generation

MHOHG [2] is a highly nonlinear nonperturbative effect resulting from two essential steps: (i) ionization at the peaks of an electromagnetic pulse $E(t)$ of maximum amplitude E_0 [Eq. (4)], followed by (ii) laser-induced recollision after 2/3 of a cycle with maximum energy of harmonics of order N_m, $N_m\omega = V_{\text{ion}} + 3.17U_p$, where V_{ion} is the IP, N_m is the order of the harmonics, and $U_p = I_0/4m\omega^2$ is the ponderomotive energy [18]. Calculations of MHOHG with ultrashort (few cycles) intense, $I_0 \geqslant 10^{14}$ W/cm^2 requires special attention to grid sizes and gauges as mentioned in recent works [33]. In the present work, the MHOHG is calculated during the dynamical propagation as follows [7]. The time-dependent dipole $\vec{d}(t) = e\int n(\vec{r},t)\vec{r}d^3r$ is recorded at time intervals $\Delta t = 0.02$ au. The power spectrum of the dipole acceleration $\ddot{d}_z(t)$ in a given direction yields to the predicted HHG spectra [33]

$$S_z(\omega) \propto |a(\omega)|^2 = \left|\int \left(\frac{d^2}{dt^2}d_z(t)\right) e^{i\omega t}dt\right|^2. \quad (7)$$

Recent works showed that the most accurate method for generating the MHOHG spectra when dealing with molecular systems [2,33] is to calculate the dipole acceleration $\ddot{d}_z(t)$ according to Ehrenfest's theorem [34]. To get an additional insight into the recollision process in the harmonic spectrum, we refer to the time profiles of harmonics obtained by a Gabor transform [2,35]

$$\ddot{d}_G(\omega,t) = \int_{-\infty}^{+\infty} \exp(-i\omega t' \int \exp\left[-\frac{(t'-t)^2}{2\sigma_0}\right]\ddot{d}(t')dt, \quad (8)$$

where $\sigma_0 = 0.1$ fs is the width of the Gaussian time window in the Gabor transform. In the frequency domain it corresponds to a Gaussian frequency filter with a spectral width equal to $10\omega_L$, where ω_L is the laser frequency ($\lambda = 800$ nm). The resulting time profile indicates the time at which the selected set of harmonics was emitted during the laser pulse [2,35].

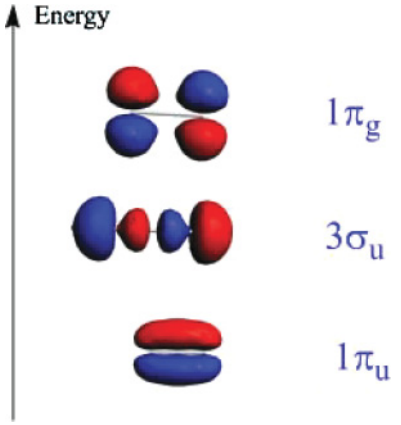

FIG. 1. (Color online) DFT images of the molecular orbitals of CO_2. Only the three highest relevant occupied molecular orbitals, HOMO, HOMO-1, and HOMO-2, are shown. Only the three highest relevant occupied molecular orbitals, HOMO, HOMO-1 and HOMO-2, are shown and energies are in Table I.

IV. RESULTS AND DISCUSSION

A. Ionization potential of molecular orbitals

One of the relevant pieces of information about the ground-state geometry of CO_2 is that the molecule is linear with an equilibrium CO bond length $R = 0.1162$ nm. The analysis of the electronic structure from the DFT-KS calculation is depicted in Fig. 1. where the three highest occupied KS molecular orbitals, HOMO, HOMO-1, and HOMO-2, with their phases are presented.

The nodal properties that correctly reflect the g and u symmetry character of the orbitals are visible. One finds that the HOMO is the antibonding $1\pi_g$, formed of π lobes lying perpendicular to the internuclear axis and located on the oxygen atoms. Table I shows the value of the IP computed as $-\varepsilon_{\text{HOMO}}$ for the LDA and the LB94 potentials. The eigenvalue of the other relevant molecular orbitals, HOMO-1 and HOMO-2, are also shown. Comparison with the experimental value [36,37] reveals that the expected underestimation of the HOMO eigenvalue at the LDA level is clearly noticeable, the computed value compared to the experimental one is approximately 43% lower. The reason for this large discrepancy lies, as mentioned in Sec. II, in the wrong asymptotic behavior of the LDA. The LB94 potential, on the other hand, performs much better, the global agreement with the experiment satisfying to within 5% of error, while results are overestimated 6% with the HF approach. The assigned electronic configuration that follows from the orbital energies is $KK(\pi_u)^4(\sigma_u)^2(\pi_g)^4$ using LDA, LB94, and $KK(\sigma_u)^2\ (\pi_u)^4(\pi_g)^4$ for HF. We note

TABLE I. Comparison of most relevant orbital binding absolute energies of CO_2 computed as $-\varepsilon_{\text{HOMO}}$ with LB94, LDA, HF, and experimental ionization potentials (in eV).

Orbital	LDA	LB94	HF	Exp[37]
$1\pi_g$ (HOMO)	9.25	13.62	14.86	13.8
$3\sigma_u$ (HOMO-1)	12.84	16.96	20.23	18.1
$1\pi_u$ (HOMO-2)	13.01	17.21	19.52	17.6

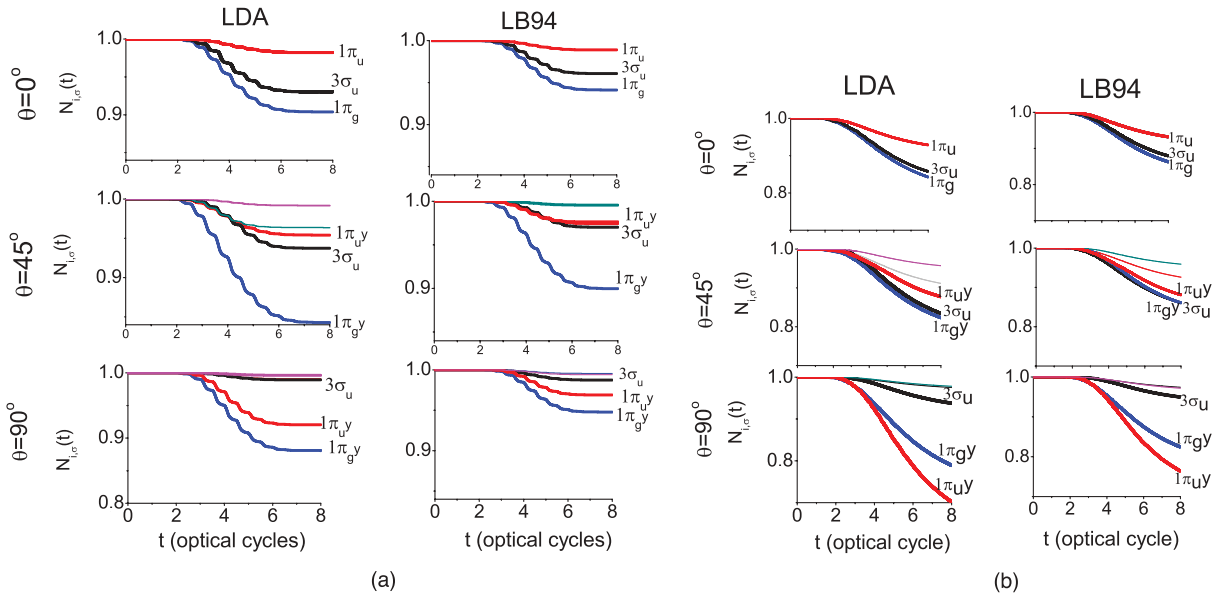

FIG. 2. (Color online) (a) TDDFT-LDA and TDDFT-LB94 orbital population, $N_{i,\sigma}(t)$, at $I_0 = 3.50 \times 10^{14}$ W/cm^2 laser peak intensity for selective fixed angle θ between the molecular axis and the laser polarization direction. Only the relevant KS orbitals that possess an important response to the laser field are shown with their labels. (b) TDDFT-LDA and TDDFT-LB94 orbital population, $N_{i,\sigma}(t)$, at $I_0 = 1.40 \times 10^{15}$ W/cm^2 laser peak intensity for selective fixed angle θ between the molecular axis and the laser polarization direction. Only the relevant KS orbitals that possess an important response to the laser field are shown with their labels.

a near-constant (∼4 eV) difference between LDA and LB94 IP's (KK is the configuration of the inner shell orbitals).

B. Orbital ionization

To gain a better understanding of the ionization dynamics, we investigated the time evolution of the KS orbital according to Eq. (6). Three angular orientations are considered $\theta = 0°$, 45°, and 90°.

Results using two laser intensities 3.50×10^{14} and 1.40×10^{15} W/cm^2 are displayed in Fig. 2(a) for LB94 and Fig. 2(b) for LDA. Evidence of a strong dependence of the KS remaining orbital population, $N_{i,\sigma}(t)$, with the laser intensity is observed. It emerges as expected that the KS orbital ionization yield is most important with the LDA functional, compared to LB94, due to its lower IP (i.e., the smaller the ionization potential of the electronic shell is the easier it can be ionized). When $\theta = 0°$, the two components of each π orbital have the same behavior for symmetry reason as they degenerate. At laser intensity $I = 3.50 \times 10^{14}$ W/cm^2, one sees that the HOMO, $1\pi_g$, molecular orbital shows, as expected, the dominant response to the laser field and is followed by the inner $3\sigma_u$, HOMO-1, the ionization for which increases steadily with the increasing laser intensities. It is therefore evident that for an intensity higher than 1.40×10^{15} W/cm^2, the HOMO will not show the dominant response to the field. Instead, the ionization of the inner $3\sigma_u$ HOMO-1 will be more important and it will exceed that of the HOMO. This is related to the symmetry of the HOMO which has a nodal plane containing the molecular axis. This gives rise to a low ionization yield when aligned parallel to the laser electric field, while the $3\sigma_u$ MO has the right symmetry (MO shape) to interact with the laser field as its density is maximum parallel to the field. No clear evidence of the ionization of the $1\pi_u$ orbital is visible. When $\theta = 45°$, the symmetry behavior of the different components of the π orbital is broken (degeneracy is removed) and renamed (e.g., $1\pi_g$ components are renamed $1\pi_g x$ and $1\pi_g y$). Independently to the potential used, our results reveal that the HOMO, $1\pi_g$, shows the dominant response to the field followed by the HOMO-1, $3\sigma_u$. At 1.40×10^{15} W/cm^2 intensity, one notices the enhancement of both the bonding $1\pi_u$ and the $3\sigma_u$ ($3\sigma_u$ is more pronounced). Once again, the KS orbitals from the LDA functional ionize faster than the LB94 potential. Finally, when $\theta = 90°$, a net difference is noticeable between the two laser intensities. While for 3.50×10^{14} W/cm^2, the HOMO $1\pi_g$ remains the most affected by the laser, it is now followed by the $1\pi_u$ HOMO-2. This behavior is again independent of the potential used. At 1.40×10^{15}W/cm^2, the ionization of the $1\pi_u$ HOMO-2 is so important that it exceeds that of the HOMO. More remarkably, the total KS orbital ionization when $\theta = 90°$ exceeds that of $\theta = 0°$. This comes from the bonding character (ionization enhancement) of the HOMO-2 $1\pi_u$, which possesses the right symmetry and maximum density to interact more properly with the laser polarized perpendicularly to the molecular axis. In conclusion, the KS orbital ionization increases from $\theta = 0°$ and reaches a maximum when the CO_2 is aligned at an angle around 45° from the direction of the laser polarization and then decreases at larger angles toward 90°. Our TDDFT calculations predict that KS orbital ionization is higher for $\theta = 90°$ than for $\theta = 0°$ with increasing laser intensity mainly due to the contribution of the bonding $1\pi_u$ HOMO-2 orbital. Although this orbital has a larger IP than the HOMO $1\pi_g$, its density dominates at 90° whereas the HOMO $1\pi_g$ has a node (zero density) at 90° in the center of the molecule. We conclude that for orbitals that have maximum density in the direction of laser polarization, such orbitals

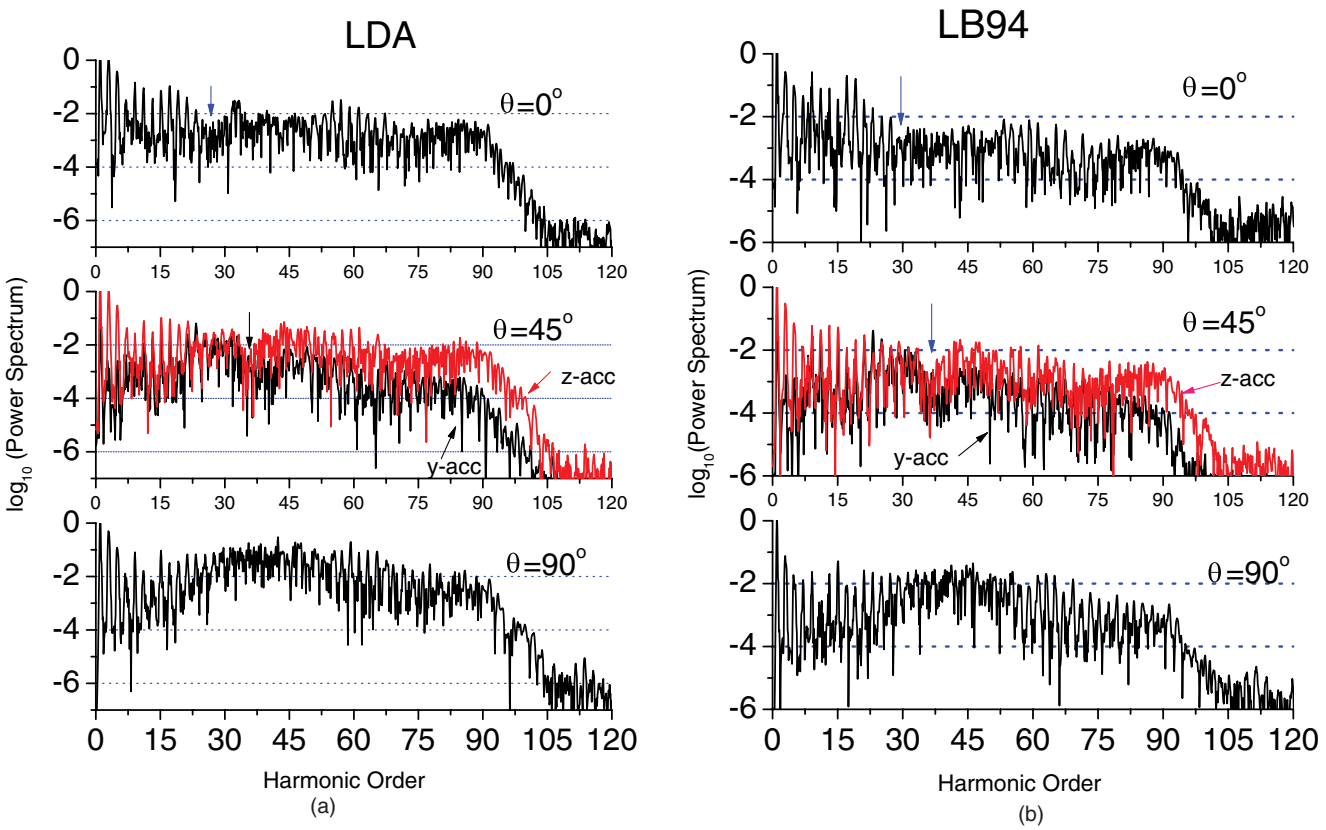

FIG. 3. (Color online) (a) TDDFT-LDA harmonic spectra for selective fixed angle θ between the molecular axis and the laser polarization direction. Laser pulse duration, eight optical cycles, peak intensity $I_0 = 3.50 \times 10^{14}$ W/cm^2, and wavelength 800 nm. (b) TDDFT-LB94 harmonic spectra for selective fixed angle θ between the molecular axis and the laser polarization direction. Laser pulse duration, eight optical cycles, peak intensity $I_0 = 3.50 \times 10^{14}$ W/cm^2, and wavelength 800 nm.

will influence or dominate in ionization and in the MHOHG processes as shown in the following.

C. Higher-order harmonic generation

In Figs. 3(a) and 3(b) , we present the MHOHG power spectra Eq. (7) emitted by CO_2 computed with the LDA and LB94 potentials. Three angular orientations of the molecule, $\theta = 0°$, 45°, and 90°, with respect to the laser-field polarization axis are considered. Calculations are done at 3.50×10^{14} W/cm^2 laser intensity. For $\theta = 45°$, the y and z components of the dipole acceleration are named, respectively, "y-acc" and "z-acc."

One finds that, in general, the overall shapes of the power spectrum resembles one another. For all orientations, features of these spectra strongly resemble those of harmonic spectra from atoms: A sharp decrease of the first few harmonics, followed by a "plateau," and ending with a cutoff that usually determines the highest harmonic order achievable and is given by the classical law $N_m\omega = V_{\text{ion}} + 3.17U_p$, as mentioned in Sec. III B. The cutoff is independent of the molecular orientation and is located approximately at the 91st harmonic, indicatingthe less sensitive effect of the ionization potential. This highest harmonic order (cutoff) does not agree with the energy cutoff formula of the semiclassical model, which is limited to ionization from a single level and IP. This is primarily due to the antibonding nature of the HOMO in CO_2 (ionization suppression) and secondly due to the contribution of the inner orbitals (i.e., $3\sigma_u$ for the case $\theta = 0°$ and $1\pi_u$ for $\theta = 45°$. This behavior was extensively discussed in other works on the O_2 molecule [38]. One notes that the lowest harmonics are hardly affected by the angle between molecules and laser-field polarization. The difference on the amplitude clearly appears when one approaches the plateau region. A minimum is observed near the 27th harmonic when $\theta = 0°$, 37th for $\theta = 45°$. To get a deep insight into the effect of the exchange correlation potential and the angular dependence on the HHG signal, we show in Figs. 4(a) and 4(b) details of the HHG from the 20th to 70th harmonic. For $\theta = 0°$, the spectrum shows the presence of a minimum signal in agreement with the experimental observation [14,16,39], but with slightly different laser peak intensities centered around the 29th harmonic for LB94 and to the 27th harmonic for the LDA.

The strength of the MHOHG signal does not increase significantly for harmonic order in the plateau independently of the potential used. This is due to the fact that the ionization rate along this direction ($\theta = 0°$) is minimal (the CO_2 HOMO is antibonding and has a nodal plane) and the minimum observed is due to a destructive resonance between the recolliding electron wave packet and the orbital. This was interpreted in terms of two center interferences between the contributions from the two atomic centers [40]. In fact, a CO_2 molecule can be regarded as an elongated diatomic molecule where the point emitters are located on the two O nuclei. When the molecular axis is 45° with respect to the laser polarization, two plots are shown following the projection of the time-dependent dipole

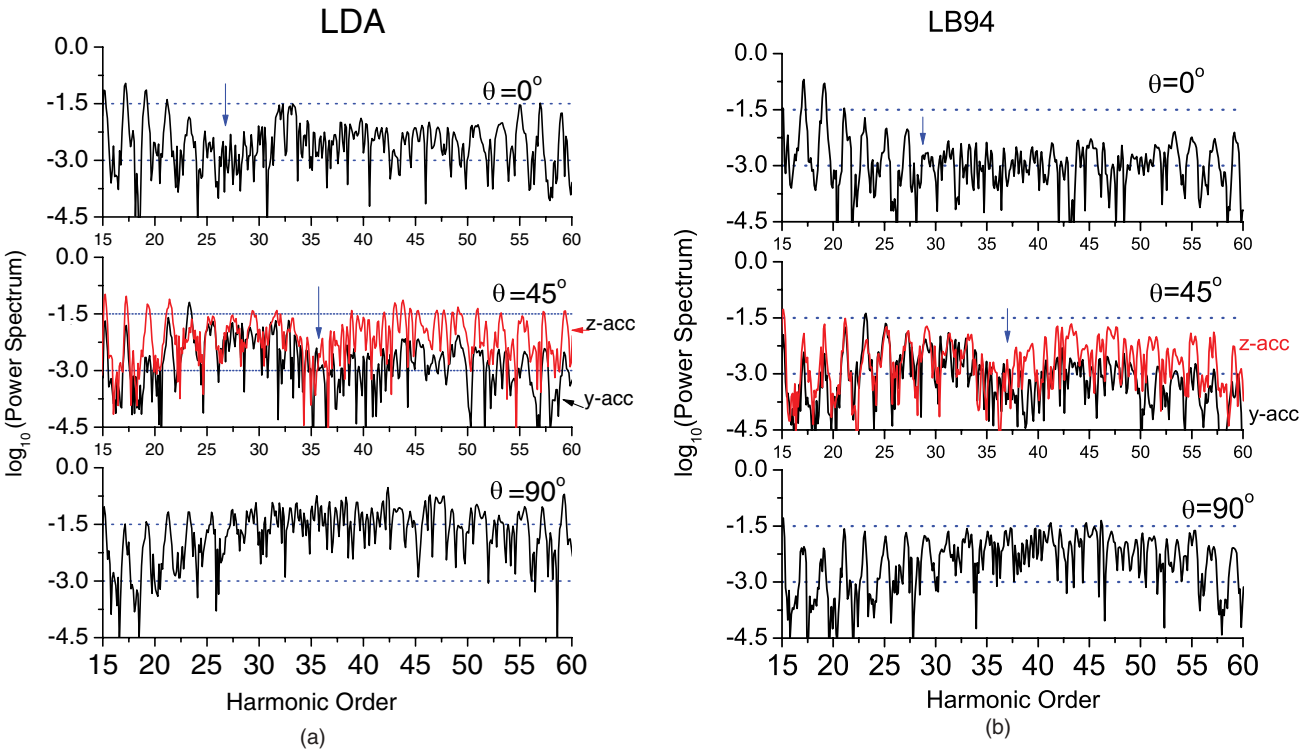

FIG. 4. (Color online) (a) TDDFT-LDA harmonic spectra in the plateau region for selective fixed harmonic orders and angle θ between the molecular axis and the laser polarization direction. Laser pulse duration, eight optical cycles, peak intensity $I_0 = 3.50 \times 10^{14}$ W/cm^2, and wavelength 800 nm. (b) TDDFT-LDA harmonic spectra in the plateau region for selective fixed harmonic orders and angle θ between the molecular axis and the laser polarization direction. Laser pulse duration, eight optical cycles, peak intensity $I_0 = 3.50 \times 10^{14}$ W/cm^2, and wavelength 800 nm.

acceleration along the z and y axes. One sees that the minimum (the destructive interference between the contributions from the two atomic centers) is shifted to the harmonic order around 35 for both. Furthermore, the MHOHG signal increases significantly compared to what is obtained at $\theta = 0^\circ$ due to the strong HOMO $1\pi_g$ orbital ionization. The stronger signal is expected because the HOMO has a maximum electron density when $\theta = 45^\circ$. The main contribution to the harmonic yield is found to be from the z component of the dipole. For $\theta = 90^\circ$, in comparison to the case $\theta = 0^\circ$, one finds that the HHG yield increases from the 20th harmonic to the 47th harmonic for the LB94 potential and the 45th for the LDA potential. Thereafter the intensity does not change significantly in the rest of the plateau domain. This is first due to the contribution of the bonding $1\pi_u$ orbital, which has a favorable symmetry to interact with the laser field (enhance the ionization) and second for a proper condition for a constructive interference between the contributions from the two atomic centers. In general, the MHOHG signal using LDA is higher compared to the LB94 potential; this is in agreement with the LDA lower IP's reported in the KS orbital ionization in Sec. III A.

To get an additional insight into the electron recombination dynamics (emission and recollision times) in the harmonic spectrum, we show for $\theta = 0^\circ$ in Fig. 5(a) the contour plots of the MHOHG time profile $\ddot{d}_G(\omega, t)$, as functions of time for harmonic orders from 40 to 100 using Eq. (8). This picture allows us to better estimate the influence of the approximation on the exchange potential and to compare our results versus the semiclassical prediction [2,22]. One can easily see that for lower-order harmonics (lower returning kinetic energy), different peaks corresponding to different electron trajectories (long and short) are visible, while higher-order harmonics refer to the electron returning to the molecular core with the maximum energy. The graph reveals that the return or recollision times for electrons with a maximum kinetic energy occurs at around 0.75of the cycle after the maximum, or the minimum of the electric field where, in fact, the field is zero in comparison to the 2/3 cycle expected from the simple three-steps model [12].

Closer inspection of Fig. 5(a) shows that lower harmonics are generated mainly by two recollisions near field extrema (i.e., at 1/8 and 5/8 cycles and at field extrema at 0 and 1/2 cycle. Highest-order harmonics are generated near field zeros, at 1/4 and 5/4 cycles. In Fig. 5(b) we show the detailed time profile of harmonics at order $N = 27$, 37, and 89 at angle $\theta = 0^\circ$. The highest-order harmonic, 89, shows a clear triple trajectory structure for both LDA and LB94 potentials. LDA is a short-range potential with no Coulomb asymptotic range, whereas LB94 is long-range as it incorporates proper Coulomb asymptotic behavior.

Nevertheless, both LDA and LB94 give rise essentially to the same recombination dynamics for the highest-order harmonic, which has the highest energy and therefore Coulomb effects are minimal. At the middle energy range, the 37th order harmonic, the LDA potential generates recollisions with less structure than LB94. Finally, for the lowest, 27th

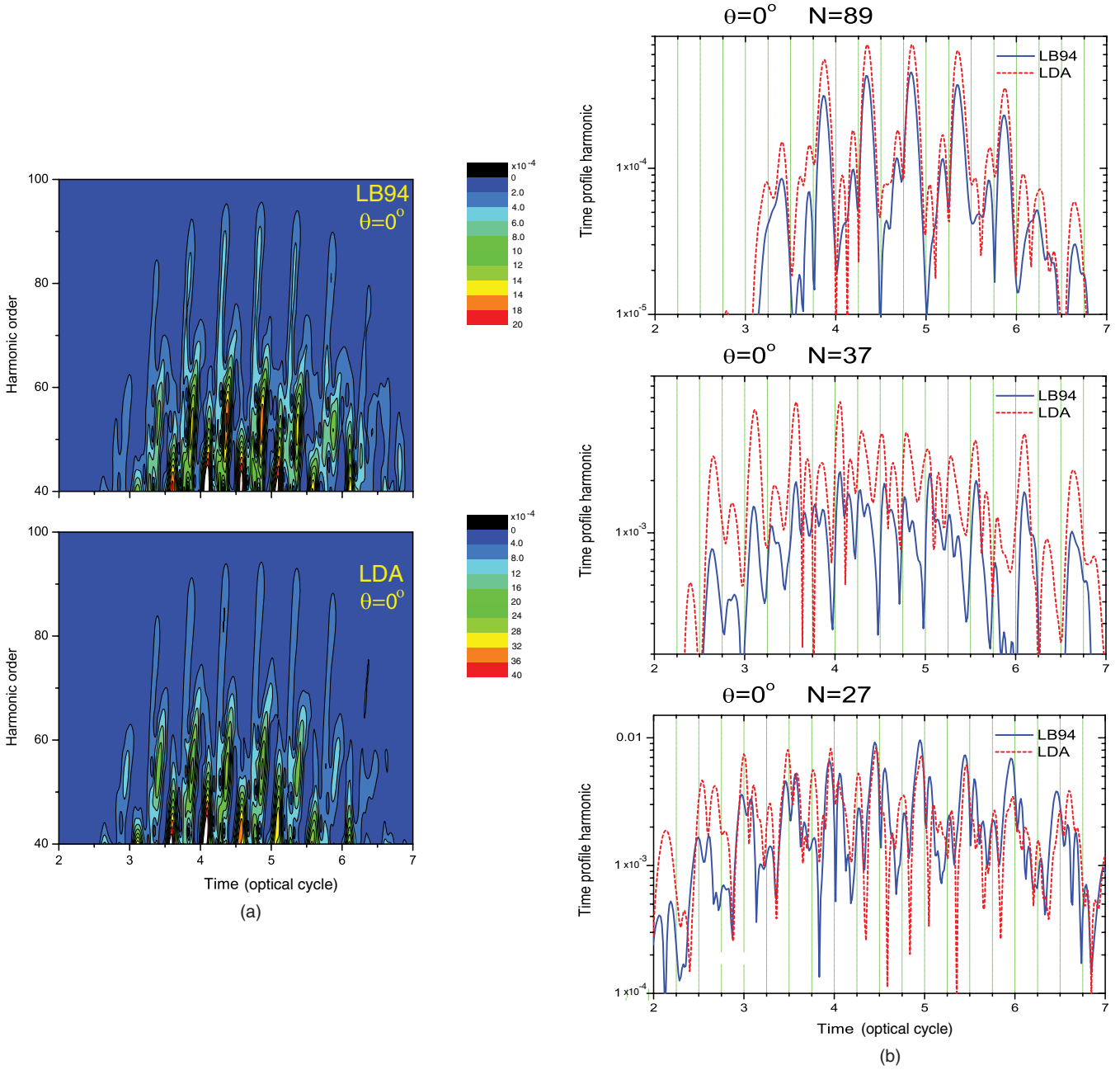

FIG. 5. (Color online) (a) Contour plot of the time profile of the acceleration $\ddot{d}_G(\omega, t)$ obtained using the Gabor time windows defined in Eq. (8). a) Top, the LB94 result is shown, b) bottom, result using LDA potential. Note that the cutoff contour is smaller with the LDA than with the LB94. $\theta = 0^\circ$, peak intensity $I_0 = 3.50 \times 10^{14}$ W/cm^2. (b) Time profile of the acceleration $\ddot{d}_G(\omega, t)$ of selected harmonics: 27th, 37th, and 89th. Results using LB94 (solid-blue) and LDA (dashed-red) are shown. $\theta = 0^\circ$ and peak intensity $I_0 = 3.50 \times 10^{14}$ W/cm^2.

harmonic, both the LDA and LB94 potentials generate, again, triple trajectories with a dominant trajectory occurring at field extrema where the electric field has maximum positive or negative amplitudes. We conclude that the short-range potential LDA generates similar recollisions in time as the Coulomb corrected LB94 potential for low and high harmonics. In the intermediate harmonic order, where LB94 produces a slight minimum in harmonic intensities [see Fig. 4(b)] more structure in recollision times for the latter potential occurs due to the presence of the Coulomb potential asymptotically.

V. CONCLUSION

TDDFT methodology was used to study the nonlinear nonpertubative response of the linear CO_2 molecule to short (few cycles) intense $I_0 \geqslant 10^{14}$ W/cm^2, 800 nm laser pulses. TDDFT allows us, due to its direct mapping into single particle states, to calculate ionization rates of individual orbitals. We thus show that for intensities at and above intensities $I_0 = 3.5 \times 10^{14}$ W/cm^2, inner-valence orbitals (i.e., lower highest occupied molecular orbitals with larger ionization potentials than the highest occupied orbital HOMO) can contribute considerably to total ionization. The main reason for this is

that these lower, inner-valence orbitals have less nodes than the HOMO and therefore for certain laser polarization the density of these lower (but higher IP) orbitals is much larger than the HOMO. Therefore, as a general rule, we note that the orbital densities determine the enhanced ionization contribution from such orbitals with increasing laser intensities. This result therefore has a strong influence on MHOHG in CO_2 since more than one orbital has a different symmetry and thus different angular density distributions will contribute to the MHOHG process. Comparison of MHOHG for a short-range potential with no Coulomb asymptotic property such as LDA with respect to the LB94 potential, which incorporates correct asymptotic Coulomb behavior, shows that Coulomb potentials broaden the minimum in MHOHG intensities as a function of harmonic order (Figs. 3 and 4). Time-series analysis based on Gabor wavelets (Fig. 5) show that a multicenter system such as CO_2, triple-electron recombination trajectories contribute to the intensity of each harmonic. It is found that the low-order harmonics are mainly generated by the recombinations of electrons at electric field extrema, where the electric field amplitudes are maximum (i.e., positive or negative). Highest-order harmonics are mainly generated by recombinations around field zeros where electric field amplitudes are weakest. This suggests that highest-order harmonics are generated when the molecule is least perturbed by the electric field, whereas lower-order harmonics are generated with both the parent ion and the neutral molecule strongly perturbed by the laser pulse.

ACKNOWLEDGMENTS

We thank the Canadian Institute for Photonic Innovations (CIPI) for support of this research through its Ultrafast Laser Science Program. We thank also Compute Canada for access to multiprocessor parallel computers for the large-scale computations reported here. Finally, we are thankful to Catherine Lefebvre, Kaijun Yuan, and Myriam Ziou for help with corrections and figure preparation.

[1] T. Brabec and F. Krausz, Rev. Mod. Phys. **72**, 545 (2000).
[2] A. D. Bandrauk, S. Barmaki, and G. LagmagoKamta, in *Progress in Ultrafast Intense Laser Science*, edited by K. Yamanouchi *et al.* (Springer, Tokyo, 2008), Vol. III.
[3] G. LagmagoKamta and A. D. Bandrauk, Phys. Rev. A **70**, 011404 (2004); **74**, 033415 (2006); M. Lein, J. Phys. B **40**, R135 (2007).
[4] T. Zuo, P. B. Corkum, and A. D. Bandrauk, Chem. Phys. Lett. **259**, 313 (1996); A. D. Bandrauk, S. Chelkowski, and I. Kawata, Phys. Rev. A **67**, 013407 (2003); M. Meckel *et al.*, Science **320**, 478 (2008).
[5] J. Itatani *et al.*, Nature (London) **432**, 867 (2004).
[6] E. Lorin, S. Chelkowski, and A. D. Bandrauk, New J. Phys. **10**, 025033 (2008).
[7] C. A. Ullrich and A. D. Bandrauk, in *Time-Dependent Density Functional Theory*, edited by M. A. L. Marques *et al.* (Springer, Berlin, 2006), p. 357.
[8] C. Lemell, X. M. Tong, F. Krausz, and J. Burgdorfer, Phys. Rev. Lett. **90**, 076403 (2003).
[9] W. Kohn, Rev. Mod. Phys. **71**, 1253 (1999).
[10] E. Runge and E. K. U. Gross, Phys. Rev. Lett. **52**, 997 (1984).
[11] A. Talebpour *et al.*, Chem. Phys. Lett. **313**, 789 (1999).
[12] P. B. Corkum, Phys. Rev. Lett. **71**, 1994 (1993).
[13] G. LagmagoKamta and A. D. Bandrauk, Phys. Rev. A **75**, 041401(R) (2007).
[14] T. Kanai, S. Minemoto, and H. Sakai, Nature (London) **435**, 470 (2005).
[15] D. Pavicic, K. F. Lee, D. M. Rayner, P. B. Corkum, and D. M. Villeneuve, Phys. Rev. Lett. **98**, 243001 (2007); X. Zhou *et al.*, *ibid.* **100**, 073902 (2008).
[16] O. Smirnova *et al.*, Nature (London) **460**, 972 (2009).
[17] P. Liu, P. Yu, Z. Zeng, H. Xiong, X. Ge, R. Li, and Z. Xu, Phys. Rev. A **78**, 015802 (2008).
[18] M. Lewenstein, P. Balcou, M. Y. Ivanov, A. L'Huillier, and P. B. Corkum, Phys. Rev. A **49**, 2117 (1994).
[19] A. D. Bandrauk and H. Z. Lu, Phys. Rev. A **72**, 023408 (2005).
[20] W. Kohn and L. J. Sham, Phys. Rev. **140**, A1133 (1965).
[21] H. O. Wijewardane and C. A. Ullrich, Phys. Rev. Lett. **100**, 056404 (2008).
[22] R. S. Mulliken, Phys. Rev. **74**, 736 (1948).
[23] A. Szabo and N. S. Ostlund, *Introduction to Advanced Electronic Structure Theory* (Dover, New York, 1996).
[24] J. F. Janak, Phys. Rev. B **18**, 7165 (1978).
[25] R. van Leeuwen and E. J. Baerends, Phys. Rev. A **49**, 2421 (1994).
[26] A. Banerjee and M. K. Harbola, Phys. Rev. A **60**, 3599 (1999).
[27] C. Toher, A. Filippetti, S. Sanvito, and K. Burke, Phys. Rev. Lett. **95**, 146402 (2005).
[28] M. E. Madjet, H. S. Chakraborty, and J. M. Rost, J. Phys. B **34**, L345 (2001).
[29] N. Troullier and J. L. Martins, Phys. Rev. B **43**, 1993 (1991).
[30] H. Jiang and I. Novak, J. Mol. Struct. **645**, 177 (2003).
[31] A. N. Hussain and G. Roberts, Phys. Rev. A **63**, 012703 (2000).
[32] F. He, C. Ruiz, and A. Becker, Phys. Rev. A **75**, 053407 (2007).
[33] A. D. Bandrauk, S. Chelkowski, D. J. Diestler, J. Manz, and K. J. Yuan, Phys. Rev. A **79**, 023403 (2009).
[34] G. LagmagoKamta and A. D. Bandrauk, Phys. Rev. A **71**, 053407 (2005).
[35] P. Antoine, B. Piraux, and A. Maquet, Phys. Rev. A **51**, R1750 (1995).
[36] S. G. Lias, in *Ionization Energy Evaluation in NIST Chemistry WebBook*, edited by P. J. Linstrom (Moscow, 1976), Vol. 69.
[37] D. W. Turner *et al.*, *Molecular Photoelectron Spectroscopy* (Wiley, London, 1970).
[38] D. Dundas and J. M. Rost, Phys. Rev. A **71**, 013421 (2005); A. Talebpour, C. Y. Chien, and S. L. Chin, J. Phys. B **29**, L677 (1996); X. Chu and S. Chu, Phys. Rev. A **70**, 061402(R) (2004).
[39] Y. Mairesse *et al.*, New J. Phys. **10**, 025015 (2008).
[40] M. Lein, N. Hay, R. Velotta, J. P. Marangos, and P. L. Knight, Phys. Rev. A **66**, 023805 (2002); M. Lein, P. P. Corso, J. P. Marangos, and P. L. Knight, *ibid.* **67**, 023819 (2003).